AAPT PHYSICS EDUCATION | AMERICAN JOURNAL of PHYSICS

# Experimental special relativity with a meter stick and a clock

M. Lund and U. I. Uggerhøj

Citation: Am. J. Phys. **77**, 757 (2009); doi: 10.1119/1.3049532
View online: http://dx.doi.org/10.1119/1.3049532
View Table of Contents: http://ajp.aapt.org/resource/1/AJPIAS/v77/i8
Published by the American Association of Physics Teachers

# APPARATUS AND DEMONSTRATION NOTES

Frank L. H. Wolfs, *Editor*

*Department of Physics and Astronomy, University of Rochester, Rochester, New York 14627*

This department welcomes brief communications reporting new demonstrations, laboratory equipment, techniques, or materials of interest to teachers of physics. Notes on new applications of older apparatus, measurements supplementing data supplied by manufacturers, information which, while not new, is not generally known, procurement information, and news about apparatus under development may be suitable for publication in this section. Neither the *American Journal of Physics* nor the Editors assume responsibility for the correctness of the information presented.

Manuscripts should be submitted using the web-based system that can be accessed via the *American Journal of Physics* home page, http://www.kzoo.edu/ajp/ and will be forwarded to the ADN editor for consideration.

## Experimental special relativity with a meter stick and a clock

M. Lund and U. I. Uggerhøj

*Department of Physics and Astronomy, University of Aarhus, DK-8000 Aarhus, Denmark*

(Received 15 November 2007; accepted 24 November 2008)

We present measurements of the velocity of electrons, performed with an apparatus using the time-of-flight method, to demonstrate that the speed of light $c$ is the limiting speed for electrons. The results obtained show the applicability of relativity in a regime where nonrelativistic physics predicts velocities exceeding $c$. The main advantages of the apparatus are the simplicity of its operation and the data analysis. By using electrons from weak radioactive sources the experiment is suitable for the undergraduate laboratory. Furthermore, we show that with electrons from a linear accelerator and the same apparatus, excellent agreement between data and the relativistic expression for the speed of electrons in the keV-MeV energy range is observed. 

[DOI: 10.1119/1.3049532]

### I. INTRODUCTION

A frequently used starting point for undergraduate books on special relativity is the observation that the speed of electrons approaches but never exceeds the speed of light $c$ as the electron energy is increased.[1–4] To achieve a difference between the relativistic electron velocity

$$v = c\sqrt{1 - \frac{1}{\left(\frac{E_{\mathrm{kin}}}{m_0c^2} + 1\right)^2}}, \tag{1}$$

and the nonrelativistic value $v_{\mathrm{nr}} = c\sqrt{2E_{\mathrm{kin}}/m_0c^2}$ of more than a few percent, electrons with energies above 100 keV must be used. In these expressions, $E_{\mathrm{kin}}$ and $m_0$ are the kinetic energy and the rest mass of the electron, respectively.

A simple apparatus to measure the velocity of electrons in the moderately relativistic regime, suitable for the undergraduate laboratory, is described. All the elements of the apparatus are easy to operate, and the data analysis is straightforward, based only on speed being defined as the distance traveled per unit time. The apparatus uses weak, 37-kBq, $^{207}$Bi, and $^{133}$Ba radioactive sources which have a half-life of 34.9 (Ref. 5) and 10.5 years,[6] respectively. These sources emit quasimonoenergetic conversion electrons of sufficient intensity to be able to carry out a measurement of the electron velocity within a few hours. Compared to other devices for the investigation of energetic electrons[7–10] our apparatus is conceptually simple. Our use of electrons from radioactive sources, instead of using electrons from a linear or Van de Graaff accelerator, makes it much simpler to operate than, e.g., the classic experiment by Bertozzi.[11] With our apparatus, knowledge of physics at the high-school level is sufficient to show that $v$ does not exceed $c$, even in the case where this is expected on the basis of the nonrelativistic expression.

### II. EXPERIMENT

The experiment is based on a measurement of the time required for the electrons to traverse the distance between two scintillator counters. To accurately measure the time of passage of keV electrons without a significant change in the electron energy, a very thin scintillator is required in the upstream end. Typically, ten scintillation photons are emitted for each keV of deposited energy, and the energy loss must be sufficient to yield enough scintillation photons to enable detection. A good and commercially available compromise is a 10 $\mu$m thick BC-400 scintillator, mounted between two 5-mm thick light guides, as shown in Fig. 1. This thickness yields a total energy loss of 6.8 for 50 keV electrons and 1.9 keV for 1 MeV electrons,[12] with a spread of similar magnitude.[13] This is a tolerable reduction of the energy of the electrons while producing sufficient scintillation light for amplification in a photomultiplier tube (PMT).

Since the combined time resolution of the two scintillators is about 1 ns, the flight path needs to be about 1 m to generate a TOF significantly larger than the time resolution. The

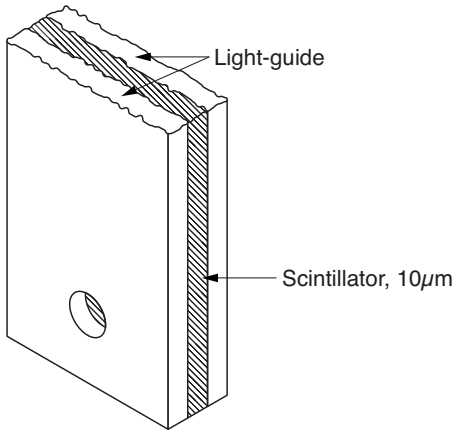


Fig. 1. A schematical drawing of the 10-$\mu$m thick scintillator and its light guides. To provide protection and stability while maintaining a high light-collection efficiency, the scintillator is located between two pieces of 5-mm thick light guides, each with a 5-mm diameter hole.

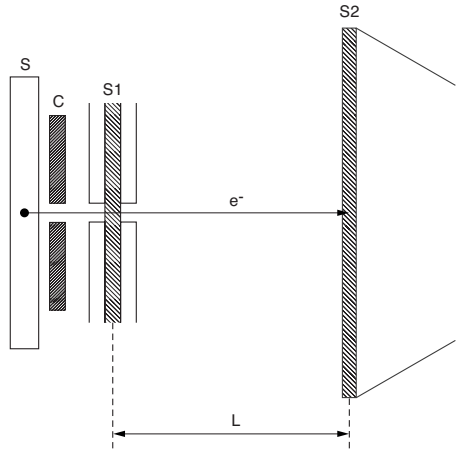


Fig. 3. A schematical drawing of the setup showing the source *S*, the collimator *C*, the 10-$\mu$m thick scintillator S1, and the 0.5-mm thick scintillator S2. Scintillators S1 and S2 are separated by a length *L*.

energy loss in 1 m of air at 1 mbar is 0.7 keV at 50 keV and 0.2 keV at 1 MeV.[12] A standard rough pump is sufficient to pump the flight path to a pressure below 1 mbar.

The experimental results discussed in this paper were obtained with the apparatus shown in Figs. 2 and 3. Both scintillators and the source were kept under vacuum, created by a turbopump. The pressure in the flight path was below $10^{-4}$ mbar.

The pulse from each scintillator triggered a "quad constant-fraction discriminator" (CFD) (ORTEC 935) which generated fast timing signals. The time difference between the fast timing signals from the S1 and S2 scintillators was measured with a "time-to-amplitude converter" (TAC) (ORTEC 567) whose output was digitized using a standard ADC card in a PC. The range of the TAC was set to 50 ns (nominal accuracy is $\pm$10 ps.) The conversion from ADC channel number to time was determined using a number of ns delays provided by an ORTEC 425A nanosecond delay (nominal accuracy $\pm$100 ps or $\pm$1%) with both start and stop derived from S1. A typical result of the time-calibration is shown in Fig. 4.

The time resolution of the electronics (including CFDs and TAC) $\delta t$ was found by splitting the signal from one PMT into the electronic chain of S1 and S2. The measured value of the time resolution ($\sigma$) in this case was 25 ps. As on the average only 20 scintillation photons are emitted from the passage of the conversion electrons from the $^{207}$Bi source through S1, statistical variations in this number results in considerable pulse-heights variations. Therefore, even though the discriminator is of the "constant-fraction" type, a rather high threshold (70 mV with −2300 V on the XP 2020 PMT, corresponding to about half the maximum amplitude) must be set. This is done to achieve good timing resolution

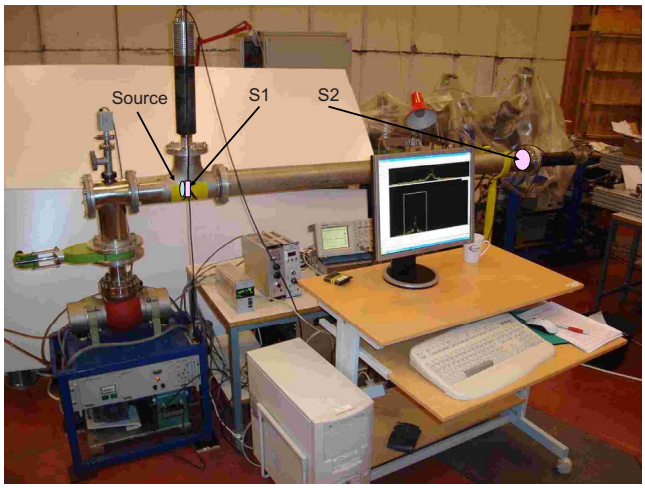


Fig. 2. (Color online) A photo of the apparatus. The source is located inside the vacuum chamber mounted on top of a turbopump. Scintillator S1, with its PMT oriented in the vertical direction, is mounted to the right of the vacuum section containing the source. At the extreme right scintillator S2 is positioned at the end of the vacuum section. The PMT of S2 is oriented in the horizontal direction.

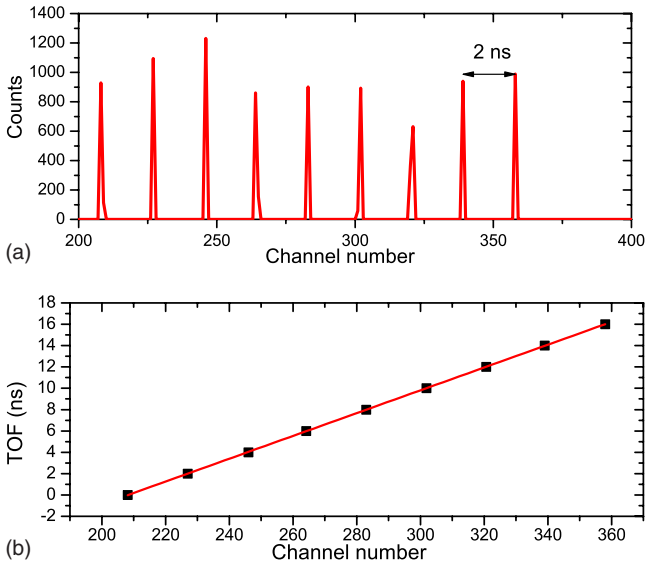


Fig. 4. (Color online) (a) Calibration spectrum of the time-to-amplitude converter using a number of 2-ns delays provided by an ORTEC 425A delay. This spectrum was obtained in about 2 min with electrons from a 37-kBq radioactive source. (b) Linear correlation between the time difference between START and STOP and the digitized output of the time-to-amplitude converter yielding a linear relationship between channel number and time $\Delta t$/channel=0.1069$\pm$0.0002 ns/channel.

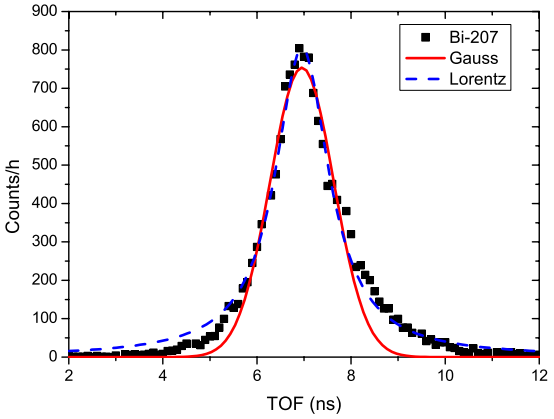


Fig. 5. (Color online) Measured time-of-flight spectrum obtained with the $^{207}$Bi source for a configuration where S1 and S2 are 5 mm apart. The curves show least-squares fits to the central region of the distribution, using a Gaussian (solid curve, $\sigma$=0.68 ns) and a Lorentzian distribution (dashed curve, $\sigma$=0.70 ns).

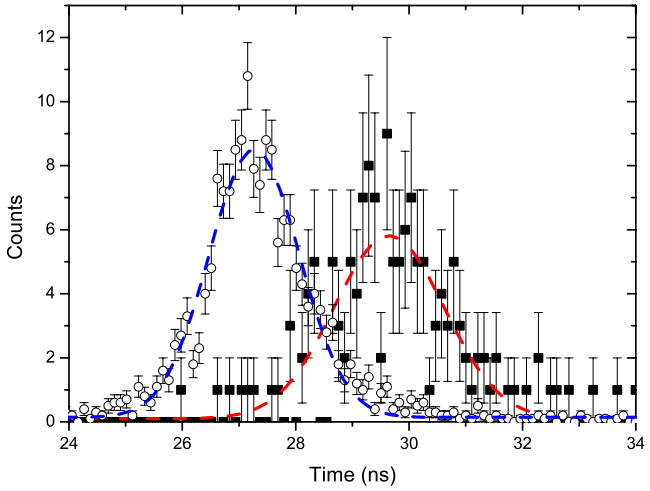


Fig. 6. (Color online) Two time-of-flight spectra obtained with the $^{207}$Bi source. The number of counts as a function of flight time in ns is shown by open circles for the configuration where S1 and S2 are spaced 5 mm apart and by filled squares for $\Delta L$=733 mm. The datataking time was 5 min in the first case (with data points scaled down by a factor 10) and 30 min in the second case. The lines show least-squares fits uisng Gaussians (dashed lines), where the shift of the centroid $\Delta t$ directly gives the velocity $v=\Delta L/\Delta t$.

and avoid an unrealistic fraction of coincidences that seem to propagate faster than the speed of light due to late triggering of S1 (this is particularly important if the setup is to be used for teaching purposes). The centroid of the distribution is unaffected by the adjustment of the CFD threshold. A reduction of the number of useful counts from the source to about half the initial value results from this threshold. Nevertheless, even with a weak, 37 kBq, $^{207}$Bi source, a useful TOF spectrum is obtained within few minutes for the configuration where the distance between S1 and S2 is 5 mm. An example of a TOF spectrum obtained with this configuration is shown in Fig. 5. The measured TOF resolution of the scintillators is $\sigma_t$=0.7 ns—PMT and scintillation by far dominating compared to the contribution from the electronics. The total number of counts obtained within an hour in this configuration is about 14 000; the centroid of the distribution can be determined with high accuracy in about 10–15 min.

The measured time between S1 and S2 includes delays due to cable lengths, CFD delays, and the actual TOF of the electrons over the flight path of length $L$. By inserting a vacuum tube of known length $\Delta L$, thus extending $L$, the observed TOF shifts by $\Delta t$, while all other parameters remain constant. The velocity is readily obtained: $v=\Delta L/\Delta t$. Figure 6 shows two typical time-of-flight spectra obtained with the $^{207}$Bi source, displaying a shift in flight time $\Delta t$ as a result of adding an extra flight path $\Delta L$=733 mm.

Covering the entire flight path of $\Delta L \simeq 1$ m in $\mu$-metal did not improve the time resolution, which means that the Earth magnetic field has no detectable effect on the measured velocity. Several thicknesses of the stop-scintillator S2 were tested, but reducing the thickness below 0.5 mm only reduces the efficiency, not the time resolution. Finally, a series of thin disks with holes, installed inside the vacuum tube and centered on the flight path, were used to determine if a substantial fraction of the electrons intercepted by S2 had been small-angle scattered off the inner wall of the vacuum chamber. Also this had no detectable effect. It is possible, however, that an intrinsically faster scintillation material like BC-418 would improve the time resolution slightly. This was not tested.

For teaching purposes it can be emphasized that the TAC is "the clock," while it is more evident to the students that a "meter stick" is needed to measure $\Delta L$. Furthermore, a discussion of the time-calibration aspects ("period" of the clock) is suitable during the insertion of the ns delays from the ORTEC 425A.

The sources used were bought from "Isotrak" with a nominal, uncalibrated activity of 37 kBq. This corresponds to approximately 0.5 $\mu$Sv/h at a distance of 0.1 m, which in most countries is acceptable for handling by students. The sources do therefore not require a source-specific licence. In a typical geometry with a 0.733 m flight path and with effective scintillator diameters of $d_{S1}$=5 mm and $d_{S2}$=90 mm, the number of coincidences within the region of interest was about 10 per minute. The energies of the main conversion electrons and their relative abundances are given in Table I. The sources are sealed with a layer of 0.9 mg/cm$^2$ aluminized

Table I. Theoretical values of energies and abundances for the main conversion electrons from $^{133}$Ba (25.5 keV is an Auger electron) and $^{207}$Bi (Ref. 14).

| Source | Energy (keV) | Abundance (%) |
|---|---|---|
| $^{133}$Ba | 25.5 | 13.9 |
| $^{133}$Ba | 43.6 | 4.0 |
| $^{133}$Ba | 45.0 | 44 |
| $^{133}$Ba | 47.5 | 1.9 |
| $^{133}$Ba | 75.3 | 7.4 |
| $^{133}$Ba | 79.8 | 1.5 |
| $^{133}$Ba | 240 | 0.34 |
| $^{133}$Ba | 267 | 0.68 |
| $^{133}$Ba | 320 | 1.31 |
| $^{207}$Bi | 481 | 21.7 |
| $^{207}$Bi | 554 | 6.0 |
| $^{207}$Bi | 975 | 100.0 |
| $^{207}$Bi | 1047 | 25.3 |

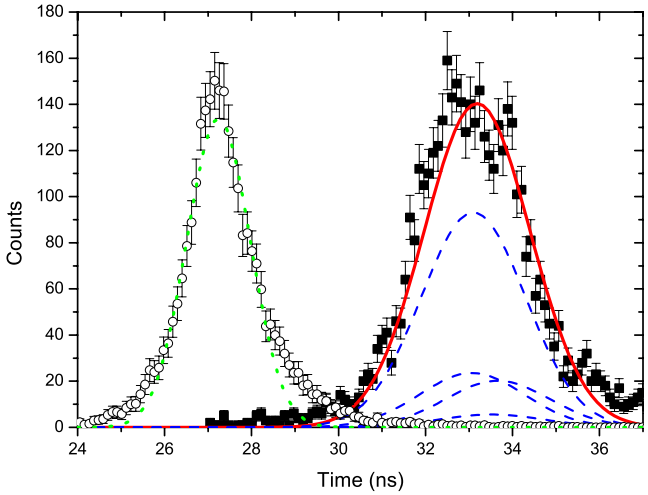


Fig. 7. (Color online) Two time-of-flight spectra obtained with the $^{207}$Bi source. The number of counts as a function of flight time in ns is shown by open circles for the configuration where S1 and S2 are spaced 5 mm apart and by filled squares at a distance with $\Delta L = 1.653$ m. The measurement with $\Delta L = 1.653$ m was taken over 93 h. The lines show least-squares fits to the distribution, using a Gaussian and a sum of four Gaussians, respectively. The four Gaussians, shown as dashed lines, are constrained by the abundances from Table I and expected flight times associated with the transition energies.

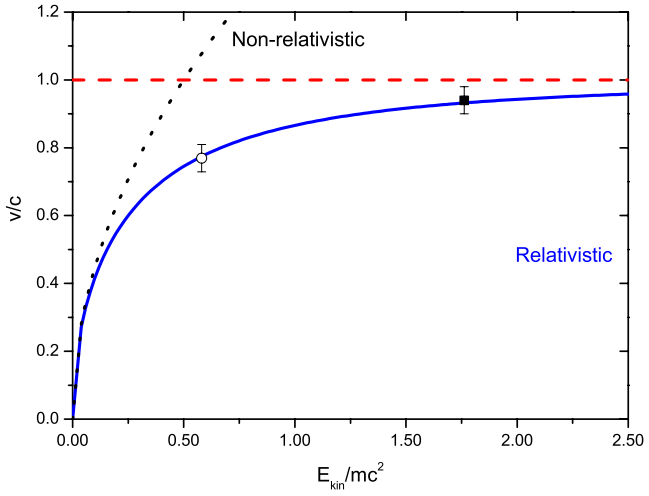


Fig. 8. (Color online) The ratio of the electron velocity and the speed of light $c$ as a function of the ratio of the kinetic energy of the electron and its rest mass $mc^2$ obtained in measurements with radioactive sources. The filled square shows a typical result obtained with conversion electrons emitted from $^{207}$Bi. A typical result obtained with a $^{133}$Ba source is shown as a circle. The solid curve shows the relativistic expression, Eq. (1), the dashed line corresponds to a velocity equal to $c$, and the dotted curve shows the nonrelativistic expression $v = \sqrt{2E_{\text{kin}}/m}$.

Mylar, covering the active region. This gives an energy loss of 2 keV at an electron energy of 1 MeV. For electron energies below 100 keV, where the difference between $v$ and $v_{\text{nr}}$ is small, the energy loss and spread through the sealing foil and S1 is comparable to the initial energy, and conversion electrons with these energies cannot be identified. For $^{133}$Ba this leaves the 240, 267, and 320 keV conversion electrons for which a TOF spectrum can be obtained (see Table I.) The sources were not damaged by residing in vacuum for extended periods of time and are thus safe to handle, with a minimum of radiation protection necessary.

## III. RESULTS

### A. Radioactive sources

With a 1-m long flight tube, the difference in the time-of-flight of and 482- and 1048-keV electrons is 0.36 ns. This difference is too small to resolve the contributing energies and a weighted average of 900 keV is used for the energy of the electrons originating from the source. Figure 7 shows a measurement with $\Delta L = 1.653$ m over 93 h—giving too low intensity for an exercise. Even in this case, the dominant contribution from the 975 keV electrons is hardly distinguishable from the contributions of the other channels.

A typical result obtained with a $^{208}$Bi source is shown in Fig. 8 as the filled square. The result, $\beta = v/c = 0.94 \pm 0.04$, clearly favours the relativistic expression by a convincingly large margin compared to the nonrelativistic $\beta_{\text{nr}} = 1.9$. This result was obtained within 2 h, including time calibration and the exchange of the flight tube with $\Delta L \simeq 0.8$ m.

A few alternative sources with a long half-life can be used: $^{137}$Cs ($E_{e^-} = 624$ keV [7.7], 656 keV [1.4]) and $^{226}$Ra ($\bar{E}_{e^-} = 172$ keV [1.8]), where only the main energies of conversion electrons are shown with the abundance in percent in the square brackets. $^{137}$Cs has the complication that there are two continuous $\beta^-$ spectra as well, with endpoint energies of 512 [94.6] and 1173 [5.4] keV. In the case of $^{226}$Ra, gamma rays, detectable in S2 with low efficiency, are emitted from a short-lived excited state in $^{222}$Ra that results from the $\alpha$ decay of $^{226}$Ra with an abundance of 5.5%. Thus, the gamma rays are emitted in close coincidence with an $\alpha$ particle that gives a strong signal in S1. With a flight tube of 1.653 m, we have measured the velocity of these photons to be $(0.99 \pm 0.01) \cdot c$.

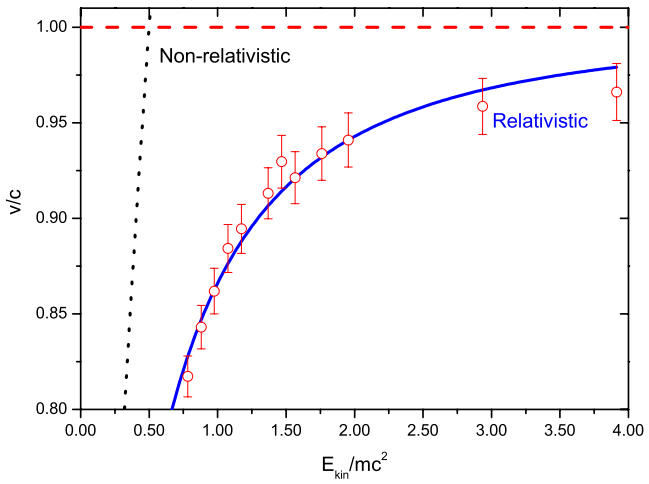


Fig. 9. (Color online) The ratio of the electron velocity and the speed of light $c$ as a function of the ratio of the kinetic energy of the electron and its rest mass $mc^2$ obtained with 400–2000 keV electrons from a linear accelerator. The full line is a curve based on the relativistic expression, Eq. (1) and the dashed line $v = c$. The dotted curve is based on the nonrelativistic expression.

### B. Linac

The experiment can also be performed with electrons from a linear accelerator (linac), using the same apparatus but with a significantly longer flight tube, i.e., a significantly reduced solid angle subtended by S2. The reduction in solid angle can be tolerated since there is no limitations on the electron intensity, and all electrons move in the forward direction. The results obtained with electrons of energies between 400 and 2000 keV are shown in Fig. 9.

As expected, these results are in excellent agreement with the relativistic expression, Eq. (1). Moreover, it is reassuring that measurements with a meter stick and a clock, used to measure flight length and time, yield results in excellent agreement with theory. Although this by no means provides a competetive test of special relativity, it does give an unequivocal demonstration of one of its most fascinating elements, that nothing moves faster than the speed of light.

## IV. CONCLUSION

We have presented measurements of the velocity of keV-MeV electrons from two weak radioactive sources showing that nonrelativistic physics ceases to be a good approximation at sufficiently high energies. The apparatus used in these measurements is suitable for the undergraduate laboratory. The results are confirmed using electrons from a linear accelerator. The measurements are essentially performed by the use of a meter stick and a clock, the basic ingredients of special relativity, and thus provide a nice and direct demonstration of a fundamental aspect of relativity.


## ACKNOWLEDGMENT

It is a pleasure to acknowledge the meticulous work of Adrian Folley at CERN in mounting the 10-$\mu$m thick scintillator which is an essential component of the apparatus.



[1] A. P. French, *Special Relativity* (W. W.Norton & Company, New York, 1968).
[2] R. Resnick, *Introduction to Special Relativity* (Wiley, New York, 1968).
[3] W. G. V. Rosser, *Introductory Special Relativity* (Taylor & Francis, London, 1991).
[4] S. Adams, *Relativity—An Introduction to Space-Time Physics* (Taylor & Francis, London, 1997).
[5] D. E. Alburger and G. Harbottle, "Half-lives of $^{44}$Ti and $^{207}$Bi," Phys. Rev. C **41**, 2320–2324 (1990).
[6] H. Schrader, "Half-life measurements with ionization chambers: A study of systematic effects and results," Appl. Radiat. Isot. **60**, 317–323 (2004).
[7] S. Parker, "Relativity in an undergraduate laboratory measuring the relativistic mass increase," Am. J. Phys. **40**, 241–244 (1972).
[8] J. G. Couch and T. K. Dorries, "Measuring relativistic electrons in the undergraduate laboratory," Am. J. Phys. **50**, 917–921 (1982).
[9] J. W. Luetzelschwab, "Apparatus to measure relativistic mass increase," Am. J. Phys. **71**, 878–884 (2003).
[10] G. J. Aubrecht II, "Comment on 'Apparatus to measure relativistic mass increase,' by John W. Luetzelschwab [Am. J. Phys. 71 (9), 878884 (2003)]," Am. J. Phys. **72**, 970–971 (2004).
[11] W. Bertozzi, "Speed and kinetic energy of relativistic electrons," Am. J. Phys. **32**, 551–555 (1964).
[12] M. J. Berger, J. S. Coursey, and M. A. Zucker, *Stopping-Power and Range Tables for Electrons, Protons, and Helium Ions* (National Institute of Standards and Technology, US Department of Commerce, Gaithersburg, MD, 1995).
[13] J. Ph. Perez, J. Sevely, and B. Jouffrey, "Straggling of fast electrons in aluminum foils observed in high-voltage electron microscopy (0.3–1.2 MV)," Phys. Rev. A **16**, 1061–1069 (1977).
[14] L. J. Jardine and C. M. Lederer, "Relative efficiency calibration of a Si(Li) electron spectrometer," Nucl. Instrum. Methods **120**, 515–520 (1974).


# Observation of standing light wave by using fluorescence from a polymer thin film and diffuse reflection from a glass surface: Revisiting Wiener's experiment


Min Sung Kim, Byeong Joo Kim, Hwan Hong Lim, and Myoungsik Cha
*Department of Physics, Pusan National University, Busan 609-735, Korea*



(Received 29 August 2008; accepted 27 October 2008)



In 1892 Drude and Nernst reported the first observation of a standing light wave by using a fluorescent thin film, which is a real-time version of Wiener's first experiment on standing light wave. We reproduce the experiment by Drude and Nernst with improved efficiency using modern laser technology and a highly fluorescent $\pi$-conjugated polymer. We also used a glass plate scratched slightly on one surface to visualize the same phenomenon using diffuse reflection instead of fluorescence. This method has the advantage of being a wavelength-independent observation compared to the fluorescence method. © *2009 American Association of Physics Teachers.*


[DOI: 10.1119/1.3027506]


## I. INTRODUCTION

When Hertz generated and measured radio waves predicted by Maxwell's equations, the observation of standing waves provided strong support for the wave theory. Soon after Hertz's pioneering experiment, Wiener demonstrated a standing wave of light.[1–3] As shown in Fig. 1(a), a silvered plane mirror was illuminated normally by a parallel beam of quasi-monochromatic light. Wiener placed a glass plate coated with a photographic emulsion layer (thinner than $\lambda/20$, where $\lambda$ is the wavelength) making a small angle of incidence. The emulsion layer was placed immediately in

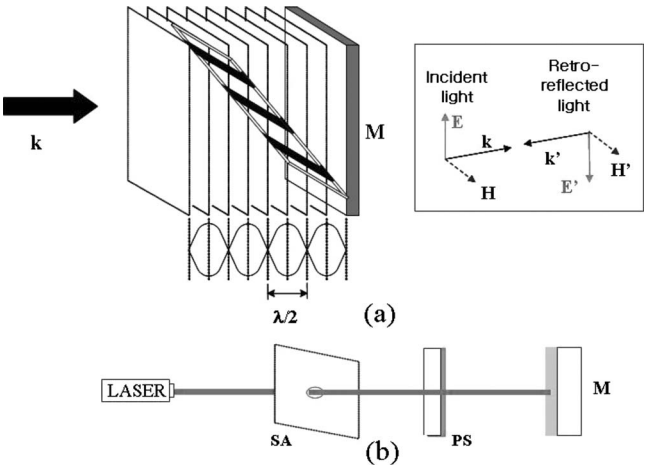


Fig. 1. Schematic diagram of (a) the original Wiener's experiment and (b) our experimental setup. The semi-transparent probing screen (PS) can be either a fluorescent thin film or a scratched glass surface. M is a silvered plane mirror. A screen with an aperture (SA) is inserted to observe the scattered light from the scratched glass. Inset: wave vectors and fields for the incident and the retro-reflected light (primed).

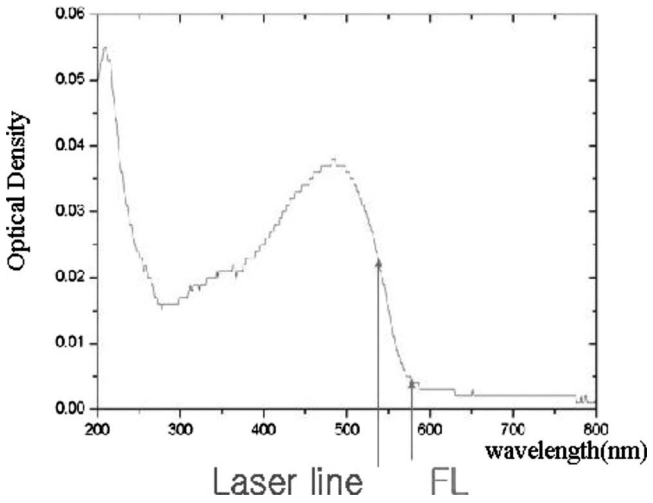


Fig. 2. Absorption spectrum for a 10 nm thick MEH-PPV film. The laser wavelength and the fluorescence center wavelength (FL) are indicated by arrows.

front of the mirror, with one edge of the slide touching the mirror surface. After developing, a series of black fringes were observed, which were due to the formation of nodes and antinodes of the standing light wave. From the fact that the first dark fringe occurred at half of the period of the fringe spacing from the contacted edge of the plate (not right at the edge), Wiener showed that the electric field in the standing light wave was responsible for the chemical change of the photographic emulsion.

A real-time observation method of standing light waves was reported by Drude and Nernst using a fluorescent thin film only a few years after Wiener's experiment.[4] The strongest fluorescence was observed when the film was placed at one of the antinodes of the electric field, and the emission was weakest between the two consecutive antinodes, where a node for the electric field was located.

We make a similar experimental demonstration to that of Drude and Nernst that can be easily implemented in an undergraduate optics laboratory. Thanks to the progress in science and technology since the original version 116 years ago, this experiment can be done with improved efficiency. In particular, we used a He–Ne laser as a light source. Lasers not only provide coherence, but also allow collimation of an intense light beam. Another improvement is the adoption of a $\pi$-electron conjugated polymer as a fluorescent material.[5] It can be easily spin-coated on a glass substrate to form a thin film with highly efficient fluorescence when excited by light with the proper wavelength. In addition, we used a precision translation stage for more direct visualization of the nodes and antinodes. We also used scattering instead of fluorescence for the standing wave observation. For this purpose a glass plate slightly scratched on one side was used in place of the fluorescent film, and the scattered light from the scratched surface was observed.

## II. OBSERVATION OF STANDING LIGHT WAVE BY FLUORESCENCE

The optical setup of our experiment is shown schematically in Fig. 1(b). We employed MEH-PPV (Sigma-Aldrich) as a probe material, which is a highly fluorescent $\pi$-electron conjugate polymer.[5] Thin films of MEH-PPV were formed on glass substrates by the spin-coating method. Three milligrams of MEH-PPV powder was dissolved in 3 ml toluene, and the solution was agitated by a magnetic stirrer for 18 h at 30 °C to make a uniform solution. The solution was dropped on an anti-reflection-coated glass substrate [Edmund-optics, B270, $MgF_2$ coated] and spun at 1200 rpm for 40 s using a spin coater [Able Co. ASS-302H]. We used an anti-reflection-coated glass substrate to reduce unwanted scattering and multiple reflections by the glass-air interfaces, although an uncoated substrate could be used for a simple demonstration. Just after coating, the film was allowed to dry for 50 s maintaining the spin rate of 800 rpm, then soft-baked at 60 °C for 30 s to evaporate the residual solvent. Under these conditions we could form 10 nm thick uniform films, with which we could resolve the changes in the fluorescence in the $\lambda/2$ range of node-to-node distance.

The absorption spectrum of the MEH-PPV thin film in Fig. 2 was measured by a spectrophotometer [Varian, Cary 5E]. Because the MEH-PPV films absorb green and emit orange light as shown in the spectrum, we used a 0.5 mW He–Ne laser operating at $\lambda = 543.5$ nm as the light source to produce standing waves. A long-wavelength pass filter was used to distinguish the fluorescence due to the film from the scattered green laser light. The filter transmits less than 0.1% of the input intensity at 560 nm and below, with the 1/2 intensity cutoff at 585 nm. The laser beam was expanded to $\approx$10 mm in diameter and collimated by a telescope to facilitate observation by the naked eye. The collimated laser beam was normally incident on a silver mirror and reflected exactly backward to make a field-superposition with the incident beam, resulting in a standing wave. A node of the electric field is formed at the mirror surface to satisfy the boundary conditions for the electromagnetic fields, and the consecutive nodal planes are located at a distance $\lambda/2$ from the mirror surface or the neighboring nodal planes.

The polymer film plane was aligned parallel to the wavefront (normal incidence), and the mirror was translated along the direction of the wavevector by a translation stage/stepping motor system [THORLABS, T25X] with a unit step

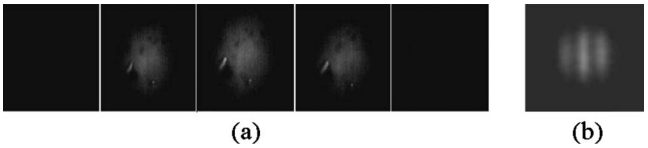


Fig. 3. Fluorescence from a polymer film from one node to the next; (a) normal incidence and (b) fringe pattern for the polymer film slightly tilted from normal incidence.

of 50 nm. Figure 3(a) shows a series of pictures taken during the translation between the adjacent nodes ($\lambda/2$ distance). Bright fluorescence is observed whenever the thin film hits an antinodal plane of the electric field. Strong absorption in the $\pi$-electron conjugate polymers is due to the electric dipole, although we did not verify that the electric field (not the magnetic field) causes fluorescence in the current experiment. Because the lifetime of the fluorescence or spontaneous emission of MEH-PPV is only a few nanoseconds, the observation of the antinodes was made in real time. No time lag of fluorescence or phosphorescence was observed when the sample was moved from an antinode to the adjacent nodes. The surface flatness of the silver mirror and the film/substrate was good enough to produce a single dark or bright pattern (without a fringe) on the film when it was within several centimeters from the mirror. This observation supports that the imperfections of the surfaces of the mirror and the substrate do not cause any wavefront aberration greater than $\lambda/2$ within the beam diameter and the round-trip distance.

We next made a slight tilt in the fluorescent film alignment, giving a small angle of incidence to visualize a few fluorescent stripes on the film as shown in Fig. 3(b). The fringe spacing became smaller with increasing angle of incidence as expected. For the three antinodes in the 1 cm beam, the tilt angle was evaluated to be $\approx 5\times 10^{-5}$ rad.

## III. OBSERVATION OF STANDING LIGHT WAVE BY SURFACE SCATTERING

A limitation of using a fluorescent polymer thin film as a sensor for standing light waves is that it suffers from photochemical bleaching after extended exposure to laser light in air. Although this limitation can be greatly alleviated by using a special packaging technique, we did not use that in our experiment. For a thin film in air exposed to a laser intensity of 1 $mW/cm^2$ or less, it took more than a few hours to lose significant fluorescence due to photobleaching. Although it did not affect the continuous demonstration of nodes and antinodes within this time scale, we found that scattering (or diffuse reflection or random diffraction) is an alternative for detecting nodes and antinodes, without the need of changing the probe material for a long time. Furthermore, He–Ne lasers producing red light ($\lambda = 632.8$ nm) are the most commonly used lasers in optics laboratories, and few fluorescent materials working at this low energy excitation are available. Although near-infrared dyes exist, the emissions are inefficient, and the result is not directly visible to the naked eye. Because scattering is not sensitive to the wavelength of the light source used in the standing wave experiment, the scattering method could be a low cost alternative to the fluorescence method in undergraduate optics laboratories, if they produce equivalent results.

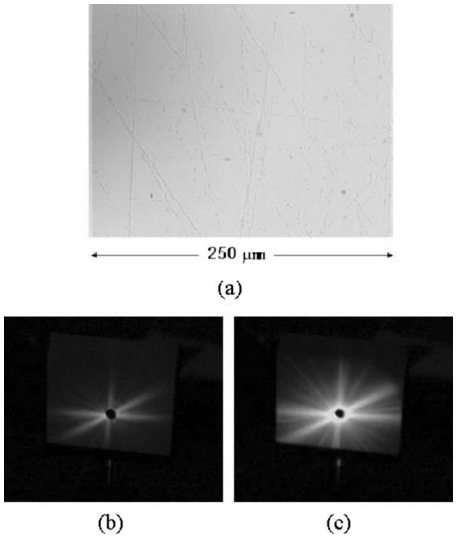


Fig. 4. Pictures of (a) a scratched surface on a glass plate, (b) the diffraction patterns from a traveling wave, and (c) a standing wave.

We made slight scratches on one surface of the same substrate as in the fluorescence experiment with a fine abrasive. Figure 4(a) shows a microscope picture of the scratched surface. The effect of the scratched surface was verified by observing the scattering of the laser beam from the surface. As shown in Fig. 1(b), a screen with a circular aperture was placed 10–20 cm before the glass plate, allowing the input beam to pass through it. The back scattered pattern on the screen was observed with and without the silver mirror. When we blocked the reflection from the mirror, only the incident traveling light wave passed through the scratched surface, causing the scattered pattern as shown in Fig. 4(b). We interpret it to be a reflected diffraction pattern due to the random gratings on the surface. In contrast, when we unblocked the reflection, allowing a standing wave to form, we observed the identical and brighter pattern shown in Fig. 4(c) if the scratched plane was properly located. Thus, the backward propagating beam produces the same diffraction pattern as in the incident beam alone, but in the transmission mode. The two patterns can interfere constructively or destructively depending on the optical path length between the scratched surface and the mirror, making the observations of nodes and antinodes possible.

The images on the scratched glass plate are comparable to those of fluorescence, although the picture quality was slightly worse due to laser speckle and the unevenly ground surface (see Fig. 5). However, nodes and antinodes were clearly distinguishable as shown in the pictures.

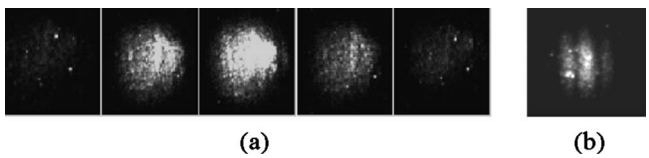


Fig. 5. Scattering from a scratched glass from one node to the next; (a) normal incidence and (b) fringe pattern when the glass plate was slightly tilted from normal incidence.

## IV. CONCLUSION AND FUTURE SUGGESTIONS

We successfully reproduced the standing wave experiment by Drude and Nernst.[4] Visualization of the nodes and antinodes was easily performed by using a laser as the light source and a fluorescent polymer or scratched glass surface as the detecting device. This experiment can be easily implemented in the undergraduate optics laboratory because of its simple setup, and there is no need for expensive equipment. The standing wave experiment utilizing the scattering method can be done with a low cost red diode laser. We also suggest that, although we used a stepping motor in this experiment, a much cheaper dc motor can be used for a classroom demonstration. Even without a motor, we can roughly see blinking on the screen by translating the sample stage manually with a micrometer screw as in the Michelson interferometers used in undergraduate optics laboratories. Our standing wave experiment is more similar to the Michelson interferometer experiment than other experiments demonstrating the wave nature of light such as Young's double slit interference and single slit diffraction, in the sense that we can directly "sense" the wavelength.


## ACKNOWLEDGMENTS

This work has been supported by Pusan National University. The authors thank Professor I. K. Yoo in our department for his help in translating Refs. 1 and 4.



[1] O. Wiener, "Stehende Lichtwellen und die Schwingungarichtung polarisirten Lichtes," Ann. Phys. **40**, 203–243 (1890).
[2] E. Hecht, *Optics*, 4th ed. (Addison-Wesley, San Francisco, 2002), pp. 288–293.
[3] M. Born and E. Wolf, *Principles of Optics*, 6th ed. (Pergamon, New York, 1989), pp. 277–281.
[4] P. Drude and W. Nernst, "Ueber die Fluorescenzwirkungen stehender Lichtwellen," Ann. Phys. **45**, 460–474 (1892).
[5] D. Braun and A. J. Heeger, "Visible light emission from semiconducting polymer diodes," Appl. Phys. Lett. **58**, 1982–1984 (1991).


# Construction of a simple spherical air bearing


M. F. Masters,[a] C. Reynolds, H. Suedhoff, and F. M. DeArmond
*Department of Physics, Indiana University-Purdue University-Fort Wayne, Fort Wayne, Indiana 46805*



(Received 29 March 2007; accepted 25 November 2008)



A simple method requiring minimal tools and mechanical ability, is presented for making a spherical air bearing. The air bearings are used for an exploration of precession. Results of test measurements are presented.



[DOI: 10.1119/1.3050161]


## I. INTRODUCTION

A number of investigations and demonstrations of rotational motion and precession can be performed using a spherical air bearing and a ball bearing or a polystyrene ball with an embedded magnet.[1–4] A billiard ball,[5] for instance, can easily be modified to contain a magnet to provide a magnetic moment. A screw, attached to the ball, can provide a gravitational torque. However, the construction of a spherical air bearing is difficult, usually requiring access to lathes and milling machines as well as experience with these tools. We have developed a very simple method for assembling a spherical air bearing as part of an effort to construct a mechanical analog of nuclear magnetic resonance.[1] Our method is inexpensive and does not require access to machines more complex than a drill press.

## II. CONSTRUCTION OF THE AIR BEARING

The air bearing is made by casting polyester resin[6] in a high-density polyethylene (HDPE), low-density polyethylene (LDPE), or polypropylene container. These types of plastic are indicated as number 2, 4, or 5 type recyclables in the United States. The advantage of these materials is that the hardened resin does not stick to them, making it easy to remove the casting from the mold. We use plastic margarine tubs as molds.

To ensure a good spherical surface, the billiard ball itself is used as part of the mold. A 1.27 cm (0.5 in.) diameter rod is hot-glued to the billiard ball. This rod supports the partially submerged ball in the polyester resin as the resin hardens. The end of the billiard ball, opposite the rod, is coated with at least three layers of poly vinyl acrylate (PVA, available in craft supply stores) as a mold release. Each layer of PVA is allowed to dry between coats. Care is taken to keep the coats of the mold release smooth and uniform, with no drips or bubbles. To make the bearing, the mold is filled to a depth of about 4 cm with polyester resin. An appropriate amount of hardener is then mixed in the mold, as described in the resin's directions. The billiard ball is suspended by the rod from a ring stand until 1–2 cm of the ball is submerged. The polyester is allowed to set for at least 24 h before the casting is removed from the mold. The billiard ball is removed from the casting using a slight twisting action.

To complete the air bearing an air orifice is required. As long as the location of the orifice is reasonably close to the center of the air bearing, its exact location will not have a measurable effect on the motion of the ball. We have varied the orifice size and found that it does not make a difference in the operation of the bearing. A 1/8 in. (3.18 mm) diameter orifice was found to work well. This orifice is partially bored through the approximate center of the casting and a second hole is bored from the side to join this first one so that a gas line can be attached to the side of the bearing, as shown in Fig. 1. The side entrance hole is bored out with a 0.332 in. drill bit and tapped for 1/8 in. pipe thread.

Modifying the billiard ball is straightforward. A cylindrical magnet can be easily embedded within the billiard ball,

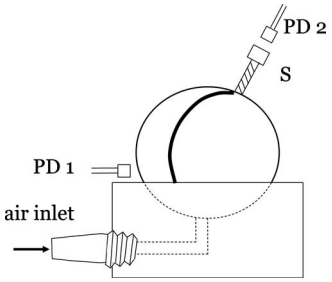


Fig. 1. Schematic of the air bearing and the experimental setup. PD1 and PD2 are small photodiodes. S is the screw with a reflective top.

using a drill press and epoxy. A gravitational torque can be generated by attaching a mass to the surface of the ball. A larger lever arm can be created by drilling and tapping a hole in the ball for an 8-32 screw. These modifications can be made prior to removing the billiard ball from the air bearing casting since the casting is a very convenient holder.

## III. OPERATIONAL DETAILS OF THE BEARING

Using a 1/8 in. orifice and an air pressure between 1 and 7 psig, the ball floats in the air bearing. All our measurements were performed with a pressure of 3 psig. Once the ball is positioned in the air bearing, it can be spun by twisting the screw by hand. For higher angular speeds, the ball can be rotated using a drill with a bit matched to the 8-32 screw.

For precession measurements with a constant external torque, it is necessary to set the angle of the axis of rotation, which lies along the direction of the screw. Once the ball is spinning, we set this angle to the desired value using an Allen wrench to change the orientation of the screw, and thus the rotation axis. To measure the angle of the axis of rotation, a desk lamp is placed on one side of the apparatus and a protractor is placed on the other. The shadow of the billiard ball and screw are projected on the protractor and the angle of the screw with respect to the vertical can be determined and held constant.

To measure frictional effects in the bearing and the precession rate of the billiard ball, it is necessary to measure

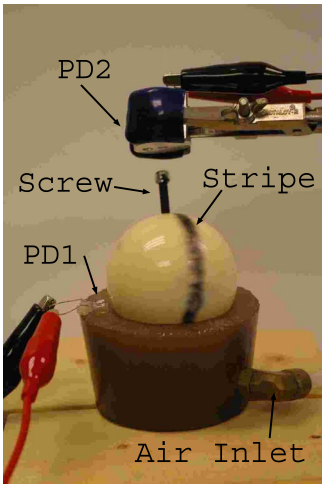


Fig. 2. Photograph of the experimental setup used to acquire the precession data. Photodiodes PD1 and PD2 are indicated.

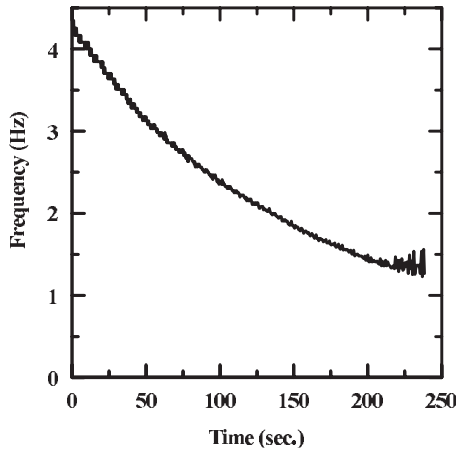


Fig. 3. Plot of the billiard ball's rotation frequency as a function of time, indicating frictional losses.

both the rotational frequency and the precession period of the ball. The rotational frequency is measured by using a small 1 $mm^2$ photodiode mounted on the edge of the bearing (PD1 in Figs. 1 and 2). A dark line is drawn half way around the ball using a black marker. As the line passes the photodiode, there is a detectable decrease in the intensity of reflected room light. The signal from this photodiode is used to determine the period of rotation of the billiard ball. To measure the precession period, aluminum foil is attached to the head of the screw. A second photodiode (PD2 in Figs. 1 and 2) is mounted at the appropriate angle such that when the screw passes under the photodiode, there is an increase in the intensity of the light reaching the photodiode. This increase in the light intensity results in a small voltage signal generated by the photodiode. The time between two or more signals from PD2 yields the precession period.

## IV. TESTING THE AIR BEARING

To test the functionality of the air bearing two studies were performed. The first study examined the frictional effects in the air bearing to determine the quality of the bearing. In these measurements, the rotational frequency of the ball was measured as a function of time. An example of the data col-

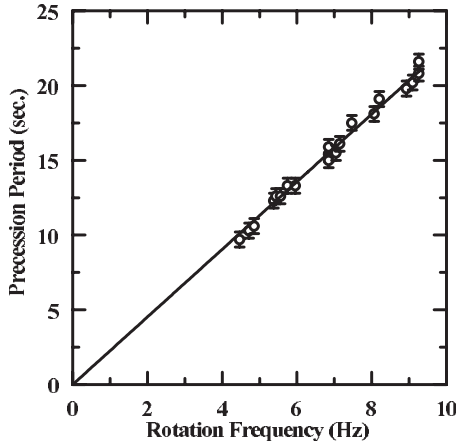


Fig. 4. Plot of the precession period vs. the rotational frequency of the billiard ball. The slope of the best fit line is $2.26 \pm 0.14$ $s^2$.

lected is shown in Fig. 3. The measured frequency shows an exponential decrease with increasing time, indicating an angular speed dependent frictional torque.[7]

The second study measured the dependence of the precession period on the angular speed of the billiard ball. To change the torque, mass was added to the screw at various distances from the ball's center. For this study, a 3.8 cm long 8-32 screw in the billiard ball and a small lead mass provided the torque (see Figs. 1 and 2). For a precession angular velocity that is small compared to the rotational velocity of the object, the relation between the precession angular velocity $\Omega_p$ and the rotational angular velocity $\omega$ of the object around its rotation axis can be written as

$$\Omega_p = \frac{m_s g R}{I\omega}, \tag{1}$$

where $m_s$ is the total mass of the screw and the lead, $R$ is the distance between the center of the ball and the center of mass of the screw and the lead, and $I$ is the moment of inertia of the ball. If we rewrite Eq. (1) in terms of the precession period $T_p$ and the rotational frequency $f$, we obtain

$$T_p = \frac{4\pi^2 I f}{m_s g R}. \tag{2}$$

Plotting the precession period as a function of the rotational frequency of the ball will result in a straight line with a slope of $4\pi^2 I/m_s g R$ and zero intercept. The best linear fit to the collected data has a slope of $2.26 \pm 0.07$ s$^2$ and zero intercept, as shown in Fig. 4. The principle contribution to the uncertainty in these measurements arises from measurement of the precession period ($\pm 0.5$ s) determined through multiple measurements of the precession period for a given rotational frequency.

Given the mass of the billiard ball ($178.4 \pm 0.1$ g) and its radius ($5.70 \pm 0.01$ cm), we can calculate its moment of inertia: $2.318 \times 10^{-4} \pm 5 \times 10^{-7}$ kg m$^2$. The center of mass of the screw and the lead is located $4.35 \pm 0.1$ cm from the center of the ball. Its total mass is $9.7 \pm 0.1$ g. The predicted slope is $2.21 \pm 0.08$ s$^2$, in good agreement with the measured slope.

## V. CONCLUSION

A simple method to construct an air bearing has been described. The cost to make the entire apparatus is less than $20. It would not be a difficult task to equip an entire undergraduate laboratory with this apparatus to investigate precession. This bearing can also be used to examine drag, as in Ref. 7, for spherical geometries. In addition, the method described in this paper can be used to make a simple air bearing for a pendulum, as in Ref. 8.


## ACKNOWLEDGMENT

This work was partially funded by NSF CCLI Grant No. 0127078.



[a]Electronic mail: masters@ipfw.edu; URL: http://users.ipfw.edu/masters.



[1]Harold A. Daw, "Two air-supported devices for physics laboratories and for physics demonstrations," Am. J. Phys. **33**, 322–326 (1965).

[2]Robert G. Marcley, "Apparatus drawings project. Report number 3. Air suspension gyroscope," Am. J. Phys. **28**, 150–155 (1960).

[3]Bernard H. Duane, "Air suspension gyroscope," Am. J. Phys. **23**, 147–150 (1955).

[4]O. L. de Lange and J. Pierrus, "Measurement of inertial and noninertial properties of an air suspension gyroscope," Am. J. Phys. **61**, 974–981 (1993).

[5]Billiard balls may be purchased for approximately $10 per ball. We prefer the cue balls without an internal magnet.

[6]Polyester resin is also known as "Fiberglass resin" and is readily available in hardware, automotive, and craft supply stores. Bondo Fiberglass Repair Kits have been our material of choice. One quart costs approximately $12 and is sufficient for about four or five bearings.

[7]B. G. Thompson and P. A. Smith, "An experiment in rotational motion with linear and quadratic drag," Am. J. Phys. **72**, 839–842 (2004).

[8]Harald C. Jensen and John R. Monahan, "Air bearing support for a pendulum," Am. J. Phys. **36**, 459–460 (1968).